IEEE Access
Multidisciplinary | Rapid Review | Open Access Journal

Received 23 September 2023, accepted 18 October 2023, date of publication 17 November 2023,
date of current version 13 December 2023.

Digital Object Identifier 10.1109/ACCESS.2023.3334274

RESEARCH ARTICLE

Formation Control of Spacecraft Based on *SE*(3) With Asymmetric Saturated Input

CHAOBO LI[1], XIAOKANG PENG[2], WEI SHANG[1], YUHAN ZOU[1], AND TIANLONG CHEN[1]
[1]School of Mechanical Engineering, Hubei University of Technology, Wuhan 430068, China
[2]Shanghai Mechanical and Electrical Engineering Institute, Shanghai 200000, China

Corresponding author: Wei Shang (bitshw@126.com)

ABSTRACT In this paper, a set of integrated control problems for distributed spacecraft formation with input asymmetric constraints under external disturbances are studied. First, a new configuration error function is designed based on the compact nonlinear manifold *SE*(3), and the dynamic model of the coupling of the orbit and attitude of the distributed spacecraft formation is established. Then, in order to ensure the thrust constraints of the spacecraft in different directions, a novel asymmetric saturation controller is designed. Secondly, to deal with the effects of non-smooth asymmetric saturation, a continuously differentiable asymmetric saturation model is used based on a Gaussian error function. Using the proposed control scheme, the desired velocity can be tracked and the desired formation created. Finally, the finite-time stability of the spacecraft formation is demonstrated using Lyapunov's stability analysis, and the effectiveness of the proposed control scheme is verified by numerical simulation results.

INDEX TERMS Formation control, spacecraft, asymmetric saturated input, *SE(3)*.

I. INTRODUCTION

Over the past few decades, formation control has become a popular area of research for many researchers and engineers. This control method dramatically improves the robustness of the system adaptability and flexibility, which has been used in many engineering tasks, such as earth observation distribution, aperture radar, gravity field measurement and so on [1], [2], [3], [4], [5]. At the same time, to meet the above requirements, the formation control technology for multiple spacecraft is also placing greater demands on the technology [6].

In the early research on spacecraft formation control, WH Clohessy [7] proposed a scheme of spacecraft formation control based on linear model. In [8], a nonlinear controller with adaptive laws is proposed in order to ensure global asymptotic convergence of the relative position and attitude errors. Subsequently, P.K.C. Wang developed a non-linear model for spacecraft formation control and designed a non-linear state feedback control method that enables asymptotic position tracking and global exponential attitude tracking. However, many practical systems usually are required to converge in finite time as the finite time control has faster convergence speed, higher control accuracy and better robustness [10], [11], [12]. In [13], based on adaptive nonsingular terminal sliding mode control, a distributed control law for satellite formation is proposed, which achieves finite time consistency. In [11], a finite-time convergent extended state observer is developed, which can estimate the external disturbance with high precision. In [14], a finite time controller with high precision convergence is proposed by applying the adaptive nonsingular fast terminal sliding mode surface, which is robust to time-varying disturbances and uncertainties. In [15], a distributed finite time controller with attitude measurement only is proposed. The tracking error is kept within the predefined feasible region to ensure the transient and steady-state performance. The finite time control of satellite formation is worthy of further study.

The aforementioned literature pertains to spacecraft with separate attitude and orbital control subsystems. Orbital control influences the spacecraft's trajectory, altitude, and

The associate editor coordinating the review of this manuscript and approving it for publication was Huaqing Li.

velocity, while attitude control affects the spacecraft's relative position and orientation with respect to its surrounding environment. Certain missions require the spacecraft to operate on specific orbits while maintaining designated attitudes to achieve mission objectives, such as optimal solar panel orientation and alignment of communication antennas. Therefore, achieving simultaneous control of attitude and orbit is imperative. However, realizing concurrent control of attitude and trajectory introduces challenges like attitude-orbit coupling, heightened precision requirements, and increased computational complexity. Presently, quaternion-based control theory has emerged as a potent tool to address the issues of attitude-orbit coupling in spacecraft. Quaternions circumvent the singularities associated with rigid body attitude descriptions, making them widely applicable in spacecraft large-angle attitude maneuvers [16], [17], [18].

Of these, dual quaternions have become an important tool in the study of individual or formation spacecraft orbit and attitude control problems, and a large body of research has been accumulated in the literature. [19], [20], [21], [22], [23]. In [19], a coupled model utilizing dual quaternions is proposed, presenting an event-triggered motion vision estimation strategy for spacecraft attitude estimation. This strategy effectively addresses model mismatch issues caused by event-triggering while reducing spacecraft energy consumption. Referring to [20], an adaptive terminal sliding mode control algorithm is introduced based on dual quaternions modeling, ultimately achieving practical stability of the spacecraft control system in a finite-time framework. In [21], within the framework of dual quaternions, an optimization of conventional spacecraft controllers is achieved using newly introduced dual quaternion direction cosine matrices.

However, there are redundancy, fuzziness and unwinding in the quaternion based attitude deployment, which does not intuitively represent the deployment to ensure the integrated attitude orbit control of formation spacecraft. The same attitude can be described by two groups of different quaternions, so it is fuzzy to describe the rigid body attitude with quaternions, which will lead to unwinding in the process of attitude control and consume too much energy stored in the spacecraft [24].

Consider the above analysis, this paper proposes a formation control scheme based on *SE(3)*. SE(3), a non-linear compact manifold with 16 elements and 10 constraints, has a more complex configuration and definition of the generalised velocity error vector than that of the Euclidean space. The modeling scheme based on SE(3) offers simple expressions and helps avoid the singularity of attitude representation [25], [26]. It meets the coordinated formation control of attitude and orbit of spacecraft, but also avoids the problems of redundancy, fuzziness and unwinding while describing the attitude position motion and its coupling effect of spacecraft. Furthermore, this modeling scheme based on SE(3) preserves the inherent geometric topology of the attitude of a rigid body, ensuring that it is not compromised.

The above research deals with the symmetrical constraints of spacecraft system. In the high altitude with complex actual situation, the spacecraft is affected by many factors such as material, space structure and load. The upper limit of bearing energy of each spacecraft in all directions is different, which leads to the asymmetric constraints of input spacecraft system.To address this challenge, we have introduced an asymmetric saturation controller. What sets this controller apart is its ability to adaptively adjust input thresholds in different directions based on the specific load characteristics of the satellite. This adaptive approach allows us to better cater to the demands of real-world applications. Moreover, our proposed control algorithm exhibits significantly enhanced convergence performance compared to previous works, providing a more reliable control solution for practical implementations.

The main innovations of this paper are as follows:

(1) A new SE(3)-based configuration error function description system is proposed, which can solve the difficult problem of spacecraft orbit-attitude coupling more effectively.

(2) In order to guarantee thrust constraints in different directions, a continuously differentiable asymmetric saturation model based on Gaussian error function is proposed, which solve the effect of non-smooth asymmetric saturation.

(3) A new finite-time control scheme that satisfies asymmetric saturated inputs is proposed for distributed formations of spacecraft, enabling the spacecraft to track the desired velocity and form the desired formation.

The rest of the paper is organized in this way. The Section II describes the geometric dynamics modeling and analysis model of spacecraft attitude orbit integration; The Section III mainly describes how to control the attitude orbit integration of spacecraft; In Section IV, the accuracy of the control method is verified by simulation language, and the error is analyzed; The Section V is the summary and prospect of this paper and it also summarizes the innovation points.

II. INERTIAL MODEL DESIGN AND ANALYSIS

A. GRAPH THEORY [27]

An undirected fix graph is denoted as $G = (\upsilon, \varepsilon)$, where $\upsilon = \{1, 2, \ldots, N\}$ and $\varepsilon \subset \upsilon \times \upsilon$ represent the node set and edge set, respectively. The edge (i, j) means node i can transmits information to j. Node j is set as the child node, node i is set as the parent node and it is a neighbor of node j. N_i represents the neighbor set of node i. A directed path from node i_1 to node i_n means a sequence of edges $\left(i_1, i_{1+k}\right)$, $k = 1, \ldots, n-1$. a_{ij} is defined as if there is an edge between nodes $a_{ij} = 1$; otherwise $a_{ij} = 0$. Furthermore, a path from node i to node j is defined as sequence of arcs $(i, i_1), (i_1, i_2), \ldots, (i_i, j)$. The Laplacian matrix of G is defined as $L = D - A$, in this formula $D = diag\,(d_1, \ldots, d_n)$ is a diagonal matrix, where $d_i = \sum_{j=1}^{n} a_{ij}$. If there exists at least one path from the

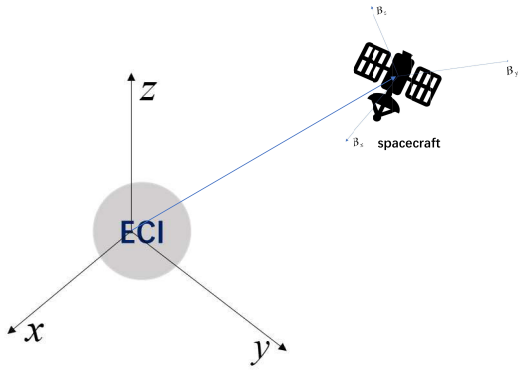

FIGURE 1. The spacecraft with body-fixed reference frames.

virtual leader to each follower, the leader is said to be globally reachable.

B. RIGID BODY DYNAMICS OF SPACECRAFT ON $SE(3)$

In this paper, the spacecraft is considered as rigid according to [32]. To define the pose of the spacecraft, assumed a coordinate frame$\{B\} = \{B_x, B_y, B_z\}$ to its body and the Earth-centered Inertial (ECI) reference frame is $\{E\} = \{E_x, E_y, E_z\}$, which is usually used to describe the absolute motion of spacecraft around the earth. As shown in Figure 1.

Let $\mathbb{R}^3$ be a three-dimensional Euclidean space at the center of mass of a rigid body. Let $p_i \in \mathbb{R}^3$ denote the i-th spcaecraft position expressed in ECI reference fram. And $R_i \in \mathbb{R}^3$ is the i-th attitude of rigid body in the frame $\{B\}$ relative to the ECI reference fram. $SO(3)$ is a Lie group and represents the rotation matrix, from the body-fixed frame to the inertial frame, which can be denoted as

$$SO(3) = \{R \in \mathbb{R}^{3\times3} | R^T R = I, \det[R] = 1\} \tag{1}$$

The Lie group $SE(3)$ is the configuration space for a rigid body motion in a 3-DOF Euclidean space, which include rotational and transnational motions. Lie group $SE(3)$ is the semi-product of $\mathbb{R}^3$ and $SO(3)$, which is described as

$$SE(3) = SO(3) \times \mathbb{R}^3 \tag{2}$$

$g_i \in SE(3)$ denotes the configurations of rigid body with respect to the inertial frame, which is expressed as

$$g_i = \begin{bmatrix} R_i & p_i \\ 0_{1\times3} & 1 \end{bmatrix} \tag{3}$$

The kinematic equation of the rigid body based on the $SE(3)$ is

$$\dot{g}_i = g_i \bar{\zeta}_i \tag{4}$$

where $\zeta \in \mathbb{R}^6$ is the generalized velocity in the body-fixed frame ζ_i, which is described as follow

$$\zeta_i = \begin{bmatrix} \Psi_i \\ v_i \end{bmatrix} \in \mathbb{R}^6 \tag{5}$$

where $\Psi_i \in \mathbb{R}^3$, $v_i \in \mathbb{R}^3$ represent the angular and translational velocities in the body-fixed frame, respectively. The expression of $\bar{\zeta}_i \in SE(3)$ is defined as

$$\bar{\zeta}_i = \begin{bmatrix} \Psi_i \\ v_i \end{bmatrix}^- \in \begin{bmatrix} \Psi_i^\wedge & v_i \\ 0_{1\times3} & 0 \end{bmatrix} \tag{6}$$

where the map $[\cdot]^- : \mathbb{R}^3 \to se(3)$ is a bijection map. $se(3) = so(3) \times \mathbb{R}^3$ and $so(3)$ are the corresponding Lie algebras of the Lie groups $SE(3)$ and $SO(3)$, respectively. $\Psi_i^\wedge \in so(3)$ is defined as

$$\Psi_i^\wedge = \begin{bmatrix} \Psi_{i1} \\ \Psi_{i2} \\ \Psi_{i3} \end{bmatrix}^\wedge = \begin{bmatrix} 0 & -\Psi_{i3} & \Psi_{i2} \\ \Psi_{i3} & 0 & -\Psi_{i1} \\ -\Psi_{i2} & \Psi_{i1} & 0 \end{bmatrix} \tag{7}$$

where $[\cdot]^\wedge : \mathbb{R}^3 \to so(3)$ denotes the skew-symmetric matrix operation, whose inverse is defined as the vee map $[\cdot]^\vee : so(3) \to \mathbb{R}^3$. Brief discussions about the skew-symmetric matrix operator $[\cdot]^\vee : \mathbb{R}^3 \to so(3)$ and its inverse operator $[\cdot]^\vee : so(3) \to \mathbb{R}^3$ are as follows. In order to make the equation $\hat{x}y = x \times y$ feasible for any $\hat{x}y = x \times yx, y \in \mathbb{R}^3$, the hat map $[\cdot]^\vee : \mathbb{R}^3 \to so(3)$ transforms a vector in $\mathbb{R}^3$ to a 3×3 skew-symmetric matrix. More explicitly, for a vector $x = [x_1, x_2, x_3]^T$, we have

$$\hat{x} = \begin{bmatrix} 0 & -x_3 & x_2 \\ x_3 & 0 & -x_1 \\ -x_2 & x_1 & 0 \end{bmatrix} \tag{8}$$

The inverse of the hat map is denoted by the vee map $[\cdot]^v : so(3) \to \mathbb{R}^3$. The properties of the hat map are shown as follows

$$\begin{aligned} \hat{x}y &= x \times y = -y \times x = -\hat{y}x \\ tr[A\hat{x}] &= \frac{1}{2} tr\left[\hat{x}\left(A - A^T\right)\right] = -x^T\left(A - A^T\right)^\vee \\ \hat{x}A + A^T\hat{x} &= \left(\{tr \cdot [A] I_{3\times3} - A\}\, x\right)^\vee \\ R\hat{x}R^T &= (Rx)^\wedge \end{aligned} \tag{9}$$

for any $x, y \in \mathbb{R}^3$, $A \in \mathbb{R}^{3\times3}$, and $R \in SO(3)$.

The dynamics equation of the rigid body based on $SE(3)$ is

$$\Pi \dot{\zeta}_i = ad^*_{\zeta_i} \Pi \zeta_i + f_i \tag{10}$$

where $\Pi \in \mathbb{R}^{6\times6}$ is the inertial parameter, which is related to the inertial matrix $J \in \mathbb{R}^{3\times3}$ and the mass $m \in R_+$ of rigid body. Π is defined as

$$\Pi = \begin{bmatrix} J & 0_{3\times3} \\ 0_{3\times3} & mI_3 \end{bmatrix} \tag{11}$$

and $ad^*_{\zeta_i} = \left(ad_{\zeta_i}\right)^T$ is the dual map of ad_{ζ_i}. The map $ad_{\zeta_i} : \mathbb{R}^6 \to \mathbb{R}^6$ is the adjoint operator and can be expressed in a matrix ad_{ζ_i}, which is descibed as follow

$$ad_{\zeta_i} = \begin{bmatrix} \Psi_i^\wedge & 0_{3\times3} \\ v_i^\wedge & \Psi_i^\wedge \end{bmatrix} \in \mathbb{R}^{6\times6} \tag{12}$$

$f_i \in \mathbb{R}^6$ denotes the resultant generalized force. According to the potential force and external disturbance, f_i is described as

$$f_i = u_i + d_i + f_{Gi} \tag{13}$$

where $u_i \in \mathbb{R}^6$ is the designed input. $d_i \in \mathbb{R}^6$ is the generalized external disturbance caused by model simplifications, parameter uncertainties and so on. $f_{Gi} \in \mathbb{R}^6$ is the generalized potential force, for example, the force caused by gravity. In addition, the generalized forces in equation (13) is rewritten as

$$\begin{aligned} f_i &= \begin{bmatrix} f_{\Psi i} \\ f_{vi} \end{bmatrix}, u_i = \begin{bmatrix} M_i \\ F_i \end{bmatrix}, \\ d_i &= \begin{bmatrix} d_{\Psi i} \\ d_{vi} \end{bmatrix}, f_{Gi} = \begin{bmatrix} M_{g_i} \\ F_{g_i} \end{bmatrix} \end{aligned} \tag{14}$$

where $f_{\Psi i} \in \mathbb{R}^3$ and $f_{vi} \in \mathbb{R}^3$ denote the resultant external torque and force in the body-fixed frame. $M_i \in \mathbb{R}^3$ and $F_i \in \mathbb{R}^3$ denote the input torque and force, respectively. $d_{\Psi i} \in \mathbb{R}^3$ is the disturbance torque and $d_{vi} \in \mathbb{R}^3$ is the disturbance force. $M_{g_i} \in \mathbb{R}^3$ and $F_{g_i} \in \mathbb{R}^3$ denote the known moment and force caused by the potential forces, such as gravity.

According to Eqs. (6), (12) and (14), the formulas (4) and (10) can be expanded and rewritten as

$$\begin{cases} \dot{R}_i = R_i \Psi_i^{\wedge} \\ \dot{p}_i = R_i v_i \\ J\dot{\Psi} = -\Psi_i \times J\Psi_i + M_i + d_{\Psi i} + M_{gi} \\ m_i \dot{v}_i = -m_i \Psi_i \times v_i + F_i + d_{vi} + F_{g_i} \end{cases} \tag{15}$$

C. THE ASYMMETRIC CONSTRAINTS CONTROL RATE

In this section, we introduce an asymmetric constraints control rate to address the issue of asymmetric, which is described as:

$$U(u_i) = U_M \times erf\left(\frac{\sqrt{\pi}}{2u_M} u_i\right) \tag{16}$$

where $U_M = (U_a + U_b)/2 + (U_a - U_b)/2 * sig(u_i)$, $U_a \geq 0$ and $U_b \leq 0$ are the known upper and lower bounds of u_i. $sig(x) = [sign(x(1)), sign(x(1)), \cdots, sign(x(n))]^T$ is the standard sign function, and $erf(\bullet)$ is a Gaussian error function. If $|U_a| = |U_b|$, the symmetric saturation model is obtained. In this paper, $|U_a| \neq |U_b|$, so we can get an asymmetric saturation actuator.

Remark 1: $U(u_i) \in \mathbb{R}^6$ is an asymmetric constraints control rate containing forces and torques. Different upper and lower bounds can be set for elements in the matrix, which can meet the force constraints of spacecraft in different directions.

in order to facilitate the derivation of the part of control design later, define following function

$$\Delta(u_i) = \begin{bmatrix} \Delta(M_i) \\ \Delta(F_i) \end{bmatrix} = U_i - u_i \tag{17}$$

The proposed saturation model can be translated into

$$U_i = \Delta(u_i) + u_i \tag{18}$$

Then, the dynamic model (15) is rewritten as

$$\begin{cases} \dot{R}_i = R_i \Psi_i^{\wedge} \\ \dot{p}_i = R_i v_i \\ J\dot{\Psi} = -\Psi_i \times J\Psi_i + \Delta(M_i) + M_i + d_{\Psi i} + M_{gi} \\ m_i \dot{v}_i = -m_i \Psi_i \times v_i + \Delta(F_i) + F_i + d_{vi} + F_{g_i} \end{cases} \tag{19}$$

Assumption 1: The communication graph among spacrcrafts is undirected and connected, and at least one spacrcraft can know the leader's states.

Assumption 2: The disturbances d_i are bounded and satisfy that $\|d_i\| < d_M$, where d_M is a positive constant and d_M is the vector of the max value of total disturbance.

Assumption 3: In practical engineering, input saturation or constraint of spacecraft control system must be considered due to the constraint of maximum actuator torque or force.

D. CONTROL OBJECTIVE

The control objective of this work is 6-DOF spacecrafts in space. The aim of this work is control multiple spacecraft to reach the desired trajectory. In the case of asymmetric constraints, the orbital motion attitude of multiple spacecrafts can be achieved consistently.

E. SOME LEMMAS

Lemma 1 ([28]): Suppose that there exists a continuous differential positive definite function $V(t)$, If the differential inequality equation (20) is satisfied by $V(t)$. Then, $V(t)$ will converge to the equilibrium point in a finite time t_f.

$$\dot{V} + \alpha V^r - \beta \leq 0 \tag{20}$$

$$t_f \leqslant \frac{1}{\alpha(1-r)} (V(0))^{1-r} \tag{21}$$

where α, β, r are real numbers, which satisfy $\alpha > 0$, $\beta > 0$, $0 < r < 1$.

III. MAIN RESULTS

Based on $SE(3)$ scheme, dynamic analysis and discussion of spacecraft errors are discussed in this section. Combined with the distributed formation control strategy, a finite time controller is designed for each spacrcraft, and the asymmetric saturation input is satisfied.

A. ERROR KINEMATICS AND DYNAMICS

The desired configurations of the i-th spacecraft relative to the reference spacecraft is $p_i \in \mathbb{R}^3$. The system dynamics model is given as follows:

$$\begin{cases} \dot{g}_j = g_j(\zeta_j)^{-} \\ \dot{\zeta}_j = \Pi^{-1}\left(ad^*_{\zeta_j} \Pi \zeta_j + U_j\right) \end{cases} \tag{22}$$

As some spacecraft can not get attitude information from leader directly, design the following sliding mode observer

$$\begin{cases} \dot{\hat{g}}_j = \hat{g}_j\left(\hat{\zeta}_j\right)^{-} \\ \prod \dot{\hat{\zeta}}_j = ad^*_{\zeta_j} \prod \zeta_j + U_j - k e_g\left(g_j, \hat{g}_j\right) \end{cases} \tag{23}$$

where $\hat{g}_j$ is the observation from the j-th spacecraft observer on $SE(3)$, which gives the the reference trajectory for each follower spacecraft in the communication graph. e_g is the configuration error vector, which specific forms are as follows:

$$\begin{aligned} e_g\left(g_j, \hat{g}_j\right) &= \begin{bmatrix} e_R\left(g_j, \hat{g}_j\right) \\ e_p\left(g_j, \hat{g}_j\right) \end{bmatrix} \\ e_R\left(g_j, \hat{g}_j\right) &= \frac{1}{2\sqrt{1 + tr\left(\hat{R}_j^T R_j\right)}}\left(\hat{R}_j^T R_j - R_j^T \hat{R}_j\right) \\ e_p\left(g_j, \hat{g}_j\right) &= R_j^T\left(p_j - \hat{p}_j\right) \end{aligned} \tag{24}$$

The proof of observer (23) is in APPENDIX A.

The relative motion error model of spacecrafts can be obtained as equation(25)

$$\begin{cases} \varphi_{R_i} = \sum_{j=0}^{n} a_{ij}\left(2 - \sqrt{1 + tr\left(\hat{R}_j^T R_i\right)}\right) \\ \varphi_{p_i} = \frac{1}{2}\sum_{j=0}^{n} a_{ij}\left\|p_i - \hat{p}_j\right\|^2 \end{cases} \tag{25}$$

where φ_{R_i} is the attitude error function on $SO(3)$, φ_{p_i} is the position error function on $\mathbb{R}^3$.

The configuration error function $\varphi_{g_i} : SE(3) \times SE(3) \to \mathbb{R}$ is summarized as follows

$$\varphi_{g_i} = \varphi_{R_i} + \varphi_{p_i} \tag{26}$$

Define the configuration error e_{g_i}, which is deduced from the gradient of the configuration error function φ_{g_i}. The angular and translational velocity error vectors are defined as $e_{R_i} : SE(3) \times SE(3) \to \mathbb{R}^6$, $e_{p_i} : SE(3) \times \mathbb{R}^6 \times SE(3) \times \mathbb{R}^6$, respectively

$$e_{g_i} = \Lambda \begin{bmatrix} e_{R_i} \\ e_{p_i} \end{bmatrix} \tag{27a}$$

$$e_{R_i} = \frac{1}{2\sqrt{1 + tr\left(\hat{R}_j^T R_i\right)}}\left(\hat{R}_j^T R_i - R_i^T \hat{R}_j\right)^{\vee} \tag{27b}$$

$$e_{p_i} = R_i^T\left(p_i - \hat{p}_j\right) \tag{27c}$$

where $\Lambda = \begin{bmatrix} \sum_{j=0}^{n} a_{ij} & 0_{3\times 3} \\ 0_{3\times 3} & \sum_{j=0}^{n} a_{ij} \end{bmatrix} \in \mathbb{R}^{6\times 6}$

Let $e_{\Psi_i} : SO(3) \times \mathbb{R}^3 \times SO(3) \times \mathbb{R}^3 \to \mathbb{R}^3$ and $e_{v_i} : SO(3) \times \mathbb{R}^3 \times SO(3) \times \mathbb{R}^3 \to \mathbb{R}^3$ denote the angular and translational velocity error vectors, respectively

$$e_{\zeta_i} = \Lambda \begin{bmatrix} e_{\Psi_i} \\ e_{v_i} \end{bmatrix} \tag{28a}$$

$$e_{\Psi_i} = \Psi_i - R_i^T \hat{R}_j \hat{\Psi}_j \tag{28b}$$

$$e_{v_i} = \left(v_i - R_i^T \hat{R}_j \hat{v}_j\right) \tag{28c}$$

where $e_{\zeta i}$ is the configuration error.

To analyze the configuration error function φ_{g_i}, by considering the configuration error vector e_{g_i} and the generalized velocity error vector e_{ζ_i}, the configuration error dynamics analysis are as follows:

$$\dot{\varphi}_{g_i} = e_{g_i} \cdot e_{\zeta_i} \tag{29a}$$

$$\dot{e}_{g_i} = G_0 e_{\zeta_i} + \sum_{i=0}^{n} a_{ij}\theta_i \tag{29b}$$

$$\dot{e}_{\zeta i} = \Lambda\Pi^{-1}\left(ad^*_{\zeta_i}\zeta_i + U_i + d_i + f_{Gi}\right) - \Lambda\dot{\alpha} \tag{29c}$$

where $G_0 = \begin{bmatrix} E_i & 0 \\ 0 & I \end{bmatrix}$ is a positive definite variable matrix, $E_i \in \mathbb{R}^{3\times 3}$ is a positive definite variable matrix.

$$E_i = \frac{\left(tr\left(\hat{R}_j^T R_i\right) I - R_i^T \hat{R}_j + 2 e_{Ri} e_{Ri}^T\right)}{2\sqrt{1 + tr\left(\hat{R}_j^T R_i\right)}} \tag{30}$$

$$\theta_i = \begin{bmatrix} 0 \\ -\Psi_i^{\wedge} e_{p_i} \end{bmatrix} \tag{31}$$

$$\dot{\alpha}_i = \begin{bmatrix} R_i^T \hat{R}_j \dot{\hat{\Psi}}_j - \hat{\Psi}_j R_i^T \hat{R}_j \hat{\Psi}_j \\ R_i^T \hat{R}_j \dot{\hat{v}}_j - \hat{\Psi}_j R_i^T \hat{R}_j \hat{v} + R_i^T \hat{R}_j \hat{\Psi}_j \hat{v}_j \end{bmatrix} \tag{32}$$

Taking into account the kinematics (4) and (10) of the rigid body dynamics system described by the equation on $SE(3)$, and on the basis of analyzing the configuration error dynamics of $SE(3)$ in Subsection III-A, the sliding mode surface is designed as

$$s_i = e_{\zeta_i} + k_1 e_{g_i}\left\|e_{g_i}\right\|^{q_1/q_2 - 1} \tag{33}$$

where k_1, q_1 and q_2 are positive odd integers and satisfy $q_1 < q_2$

Derive the above formula to get

$$\begin{aligned} \dot{s}_i &= \dot{e}_{\zeta_i} + k_1\left(I + (q_1/q_2 - 1)\frac{e_{g_i} e_{g_i}^T}{\left\|e_{g_i}\right\|^2}\right)\left\|e_{g_i}\right\|^{q_1/q_2 - 1}\dot{e}_{gi} \\ &= k_1\left(I + (q_1/q_2 - 1)\frac{e_{gi} e_{gi}^T}{\left\|e_{gi}\right\|^2}\right)\left\|e_{gi}\right\|^{q_1/q_2 - 1}\dot{e}_{gi} \\ &\quad + \Lambda\Pi^{-1}\left(ad_{\zeta}^T \Pi\zeta + U_i + d_i + f_{Gi}\right) - \Lambda\dot{\alpha}_i \\ &= a + bU_i \end{aligned} \tag{34}$$

$$\begin{aligned} a &= k_1\left(I + (q_1/q_2 - 1)\frac{e_{g_i} e_{g_i}^T}{\left\|e_{g_i}\right\|^2}\right)\left\|e_{g_i}\right\|^{q_1/q_2 - 1}\dot{e}_{g_i} \\ &\quad + \Lambda\Pi^{-1}\left(ad_{\zeta}^T \Pi\zeta + d_i + f_{Gi}\right) - \Lambda\dot{\alpha} \end{aligned} \tag{35a}$$

$$b = \Lambda\Pi^{-1} \tag{35b}$$

Substituting (13) into (34), we have

$$\dot{s}_i = a + b\left(\Delta\left(u_i\right) + u_i\right) \tag{36}$$

B. CONTROLLER DESIGN

Accoring to the spacecraft relative motion error model equation (25), the spacecraft synchronization controller is designed as

$$u_i = -\beta_i \|s_i\|^{\frac{1}{2}} sig\,(s_i) + \upsilon_i \tag{37}$$

where $\beta_i \in \mathbb{R}^6$is an adaptive gain and $\upsilon_i \in \mathbb{R}^6$ are as follow

$$\dot{\beta}_i = \begin{cases} \omega_{1i}\sqrt{\dfrac{\gamma_{1i}}{2}} & \|s_i\| \neq 0 \\ 0 & \|s_i\| = 0 \end{cases} \tag{38a}$$

$$\dot{\upsilon}_i = -\frac{\lambda_i}{2} \cdot sig\,(s_i) \tag{38b}$$

in which γ_{1i} is a constant and $\omega_{1i} \in \mathbb{R}^6$ is a matrix.

$$\lambda_i = 2\varepsilon_i\beta_i \in \mathbb{R}^6 \tag{39}$$

where ε_i is a constant.

In this section, for facilitating Lyapunov stability analysis, we introduce a new state quantity. The form is as follows

$$z = \begin{bmatrix} z_1 & z_2 \end{bmatrix}^T = \begin{bmatrix} \|s_i\|^{\frac{1}{2}} sig\,(s_i) & \upsilon_i \end{bmatrix}^T \tag{40}$$

The time derivative of equation (40) is given by

$$\dot{z}_1 = \frac{1}{2\,\|z_1\|}\left(-\beta_i b z_1 + z_2 + a_1\right) \tag{41a}$$

$$\dot{z}_2 = -\frac{\lambda b}{2\,\|z_1\|} z_1 \tag{41b}$$

where $a_1 = \rho_1 z_1$. Thus, the equation can be rewritten in a vector-matrix format

$$\begin{bmatrix} \dot{z}_1 \\ \dot{z}_2 \end{bmatrix} = A \begin{bmatrix} z_1 \\ z_2 \end{bmatrix} \tag{42}$$

where $A = \frac{1}{2\|z_1\|}\begin{bmatrix} -(\beta_i b - \rho_1) & \varpi(1) \\ -\lambda_i b & \varpi(0) \end{bmatrix}$ is a bounded function so that $0 < \|\rho_1\| \leq \delta_1$, $\varpi(x)$ is a function defined as $\varpi(x) = \begin{bmatrix} x & x & x & x & x \end{bmatrix}^T$.

Theorem 1: Consider the configuration error dynamics (25). Suppose that Assumption 1 holds, the proposed force command (37) guarantees that system converge to small sets around zero in a finite time.

Proof. The Lyapunov function at this step is designed as follows:

$$V = z^T P z + \frac{1}{2\gamma_{1i}}\left(\beta_i - \beta_i^*\right)^T\left(\beta_i - \beta_i^*\right) + \frac{1}{2\gamma_{2i}}\left(\lambda_i - \lambda_i^*\right)^T\left(\lambda_i - \lambda_i^*\right) \tag{43}$$

where $\beta_i^* > 0$, $\lambda_i^* > 0$ are some constants. P is a positive definite matrix, represented by $P = \begin{bmatrix} \sigma + 4\varepsilon_i^2 & -2\varepsilon_i \\ -2\varepsilon_i & 1 \end{bmatrix}$, where $\sigma = diag\{\sigma_1, \ldots, \sigma_n\}$.

Meanwhile, for the convenience of proof, we divide equation (19) into two parts

$$V = V_0 + V_1 \tag{44}$$

where

$$V_0 = z^T P z \tag{45}$$

$$V_1 = \frac{1}{2\gamma_{1i}}\left(\beta_i - \beta_i^*\right)^T\left(\beta_i - \beta_i^*\right) + \frac{1}{2\gamma_{2i}}\left(\lambda_i - \lambda_i^*\right)^T\left(\lambda_i - \lambda_i^*\right) \tag{46}$$

in which β_i have a minimal eigenvalue, design a positive definite matrix $\tilde{Q}$,

$$\tilde{Q} = \begin{bmatrix} \tilde{Q}_{11} & \tilde{Q}_{12} \\ \tilde{Q}_{21} & 4\varepsilon_i\varpi(1) \end{bmatrix} \tag{47}$$

where

$$\tilde{Q}_{11} = 4\varepsilon_i b\left(2\varepsilon_i\beta_i - \lambda_i\right) - 2\left(\sigma + 4\varepsilon_i\varepsilon_i^T\right)\rho_1 + 2\sigma\beta_i b + \varepsilon_i\rho_2 \tag{48a}$$

$$\tilde{Q}_{12} = \left(\lambda_i b - 2\varepsilon_i\beta_i b - \sigma\varpi(1) - 4\varepsilon_i^2\varpi(1)\right) + 2\varepsilon_i\rho_1 = \tilde{Q}_{21} \tag{48b}$$

The derivative of equation (48) yields the following expression

$$\dot{V} = \dot{V}_0 + \dot{V}_1 = \dot{V}_0 + \frac{1}{\gamma_{1i}}\left(\beta_i - \beta_i^*\right)^T\dot{\beta}_i + \frac{1}{\gamma_{2i}}\left(\lambda_i - \lambda_i^*\right)^T\dot{\lambda}_i \tag{49}$$

where

$$\dot{V}_0 = z^T\left[A^T P + PA\right]z \leq -\frac{1}{2\,\|z_1\|}z^T\tilde{Q}z \leq -\frac{\varepsilon}{\|z_1\|}\|z\|^2 \tag{50}$$

$$\lambda_{\min}(P)\,\|z\|^2 \leq z^T P z \tag{51}$$

where

$$\|z\|^2 = z_1^2 + z_2^2 = \|s_i\| + z_2^2 \tag{52}$$

It can derive as follow

$$\|z\| \leq \frac{V_0^{\frac{1}{2}}}{\lambda_{\min}^{\frac{1}{2}}(P)} \tag{53}$$

and $\|z_1\| \leq \|z\|$

Then

$$\dot{V}_0 \leq -\varepsilon_i\|z\| \leq -rV_0^{\frac{1}{2}} \tag{54}$$

where $r = \frac{\varepsilon_i}{\lambda_{\min}^{\frac{1}{2}}(P)}$.

In view of the above assumption, it can be reduce to the following

$$\dot{V} \leq -rV_0^{\frac{1}{2}} + \frac{1}{\gamma_{1i}}\varepsilon_\beta\dot{\beta}_i + \frac{1}{\gamma_{2i}}\varepsilon_\lambda\dot{\lambda}_i + \frac{\|\varepsilon_\beta\|}{\sqrt{2\gamma_{1i}}}\omega_{1i}$$

$$+\frac{\|\varepsilon_\lambda\|}{\sqrt{2\gamma_{2i}}}\omega_{2i}-\frac{\|\varepsilon_\beta\|}{\sqrt{2\gamma_{1i}}}\omega_{1i}-\frac{\|\varepsilon_\lambda\|}{\sqrt{2\gamma_{2i}}}\omega_{2i}$$
$$\leq -\eta V^{\frac{1}{2}}+\frac{1}{\gamma_{1i}}\varepsilon_\beta\dot{\beta}_i+\frac{1}{\gamma_{2i}}\varepsilon_\lambda\dot{\lambda}_i+\frac{\|\varepsilon_\beta\|}{\sqrt{2\gamma_{1i}}}\omega_{1i}$$
$$+\frac{\|\varepsilon_\lambda\|}{\sqrt{2\gamma_{2i}}}\omega_{2i} \tag{55}$$

where $\eta = min\,(r, \|\omega_{1i}\|_{\min}, \|\omega_{2i}\|_{\min})$, $\|\omega_{1i}\|_{\min}$, $\|\omega_{2i}\|_{\min}$ represent the smallest item in ω_{1i}, ω_{2i}, $\varepsilon_\beta = (\beta_i - \beta_i^*)^T$, $\varepsilon_\lambda = (\lambda_i - \lambda_i^*)^T$, respectively. There exist positive constants β_i^* and λ_i^* satisfying $\beta_i - \beta_i^* < 0$ and $\lambda_i - \lambda_i^* < 0$, then, we can get

$$\zeta = \frac{1}{\gamma_{1i}}\varepsilon_\beta\dot{\beta}_i+\frac{1}{\gamma_{2i}}\varepsilon_\lambda\dot{\lambda}_i+\frac{\omega_{1i}}{\sqrt{2\gamma_{1i}}}\|\varepsilon_\beta\|+\frac{\omega_{2i}}{\sqrt{2\gamma_{2i}}}\|\varepsilon_\lambda\|$$
$$= -\|\varepsilon_\beta\|\left(\frac{1}{\gamma_{1i}}\dot{\beta}_i-\frac{\omega_{1i}}{\sqrt{2\gamma_{1i}}}\right)$$
$$-\|\varepsilon_\lambda\|\left(\frac{1}{\gamma_{2i}}\dot{\lambda}_i-\frac{\omega_{2i}}{\sqrt{2\gamma_{2i}}}\right) \tag{56}$$

The following proof is given in both cases.

Case 1). Suppose that $s_i \neq 0$, $\dot{\beta}_i = \omega_{1i}\sqrt{\frac{\gamma_{1i}}{2}} > 0$, there is always $\beta_i > 0$ for $t \in [0, +\infty)$.

When $\zeta = -\|\varepsilon_\lambda\|\left(\frac{1}{\gamma_{2i}}\dot{\lambda}_i - \frac{\omega_{2i}}{\sqrt{2\gamma_{2i}}}\right)$, let $\dot{\lambda}_i = 2\varepsilon_i\dot{\beta}_i = \omega_{2i}\sqrt{\frac{\gamma_{2i}}{2}}$, then we can obtain $\dot{\lambda} = 2\varepsilon_i\dot{\beta}_i = \omega_{2i}\sqrt{\frac{\gamma_{2i}}{2}}$.

Thus, $\zeta = 0$ and (55) is reduced to

$$\dot{V} \leq -\eta V^{\frac{1}{2}} \tag{57}$$

Case 2). Suppose that $s_i = 0$ and $\dot{\beta}_i = 0$, so $\beta_i = \beta_i^*$, $\zeta = 0$, hence

$$\dot{V} \leq -\eta V^{\frac{1}{2}}. \tag{58}$$

Now, the system is stable on the sliding surface $s_i = 0$, obtain

$$e_{\zeta_i} = -k_2 e_{g_i}\|e_{g_i}\|^{q_1/q_2-1} \tag{59}$$

where k_2 is a positive constant.

Design the Lyapulov function V_2 as follows:

$$V_2 = \varphi_{g_i} = \varphi_{R_i} + \varphi_{p_i} \tag{60}$$

Deriving V_2 with respect to time:

$$\dot{V}_2 = e_{g_i}\cdot e_{\zeta_i}$$
$$= e_{g_i}\cdot\left(-k_2 e_{g_i}\|e_{g_i}\|^{q_1/q_2-1}\right)$$
$$= -k_2\left(\|e_{g_i}\|^2\right)^{\frac{q_1/q_2+1}{2}} \tag{61}$$

From the relationship among e_{g_i}, e_{R_i} and e_{p_i}, we have

$$\|e_{g_i}\|^2 = \|e_{R_i}\|^2 + (\sum_{j=0}^{n} a_{ij}\|e_{p_i}\|)^2$$
$$\geq \frac{1}{2}\varphi_{R_i} + 2\varphi_{p_i}$$
$$\geq \frac{1}{2}(\varphi_{R_i} + \varphi_{p_i})$$
$$= \frac{1}{2}V_2 \tag{62}$$

hence

$$\dot{V}_2 \leq -\frac{k_1}{2^{\frac{q_1/q_2+1}{2}}}(V_2)^{\frac{q_1/q_2+1}{2}} \tag{63}$$

To prove to complete.

Remark: The control parameter selections in this section are as follows: Increasing $\omega_{1i}, \gamma_{1i}, k_1, q_1, q_2$ and decreasing k_2 can increase the convergence rate. However, this may lead to larger initial control inputs, which could potentially result in actuator saturation.

IV. SIMULATION

In this section, the simulation experiment for the proposed control law (37) is carried out. Numerical simulations are conducted to verify the efficacy of the asymmetrically finite-time sliding mode controllers in this paper, and their performance is compared with finite-time super-twisting sliding mode controllers. Consider a scenario with four spacecrafts, and Figure 2 illustrates the trajectory of each spacecraft, depicting their movement from the initial position to the final position. It also showcases the communication flow from S1 to S2, then to S3, and finally to S4..

A. PARAMETER SETTING

The parameters of the rigid bodies are considered to be $m = 56.7kg$, $J = diag\,(4.85\ 5.10\ 4.76)\,kg\cdot m^2$. Consider the Earth's oblateness to the level of $J2$ and the coupled relationship between the translational and rotational motion, the moments M_{gi} and forces F_{gi} induced by gravity in the body-fixed frame are acquired from the reference [29].

$$M_{gi} = 3\left(\frac{\mu}{||p_i||^5}\right)\hat{b}_i J b_i \tag{64}$$

$$F_{gi} = F_{J2} - \left(\frac{m_i\mu}{||p_i||^3}\right)b_i - 3\left(\frac{\mu}{||p_i||^5}\right)J_1 b_i$$
$$+\frac{15}{2}\left(\frac{\mu b_i^T J b_i}{||p_i||^7}\right)b_i \tag{65}$$

where $b_i = R_i^T p_i$, $J_1 = trace\,(J)\,I + J$. $\mu = 398600.44km^3s^{-2}$ is the gravitational constant of the Earth. The perturbation caused by the Earth's oblateness F_{J2} expressed in ECI frame is given as follows

$$F_{J2} = -m_i R_i^T \frac{3J_2\mu R_e^2}{2\|p_i\|^5}\begin{bmatrix} p_{ix}\left(1-\frac{5p_z^2}{\|p_i\|^2}\right) \\ p_{iy}\left(1-\frac{5p_z^2}{\|p_i\|^2}\right) \\ p_{iz}\left(3-\frac{5p_{iz}^2}{\|p_i\|^2}\right)\end{bmatrix} \tag{66}$$

where p_{ix}, p_{iy} and p_{iz} are the components of p_i, $J_2 = 0.00108263$, $R_e = 6378.14km$ is the equatorial radius of the Earth. The initial conditions (attitude and position) for each spacecraft are considered as follow: $p_1 = [0\ 100\ 10]^T$, $p_2 = [-30\ 80\ -5]^T$, $p_3 = [-20\ 60\ 0]^T$, $p_4 = [20\ 90\ 10]^T$, the formation distance D is selected as $D_{12} = [15\ 0\ 0]^T$,

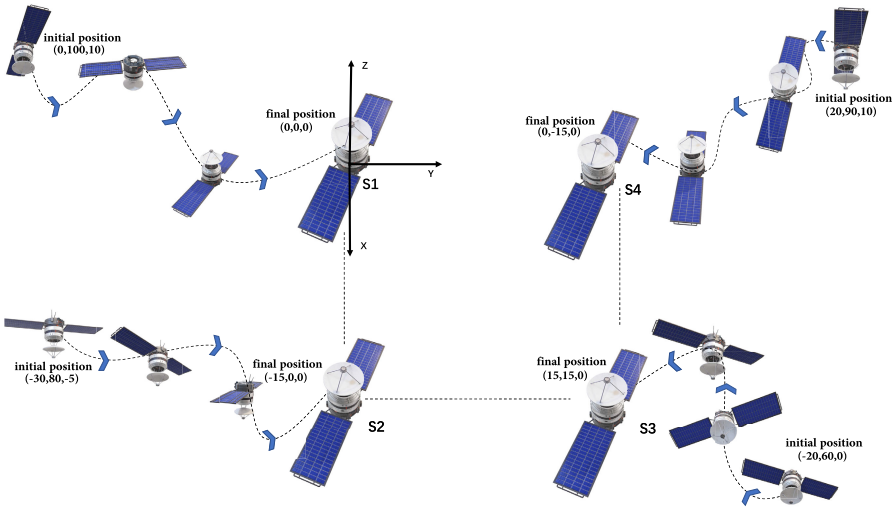

FIGURE 2. The trajectories and communication graph of the spacecraft formation.

$D_{23} = [0\ 15\ 0]^T$, $D_{34} = [-15\ 0\ 0]^T$. Furthermore, the initial velocity and angular velocity of spacecrafts are $v_1 = [0.3\ -0.2\ 0.4]^T$, $v_2 = [0.3\ -0.2\ 0.4]^T$, $v_3 = [0.2\ -0.1\ 0.3]^T$, $v_4 = [-0.3\ -0.2\ 0.2]^T$, $\Psi_1 = [0.05\ -0.03\ -0.04]^T$, $\Psi_2 = [0.05\ -0.03\ -0.04]^T$, $\Psi_3 = [0.01\ -0.02\ -0.02]^T$, $\Psi_4 = [-0.03\ \ 0.03\ -0.01]^T$. The desired formation of the position, velocity, and angular velocity are set as $p_d = [0\ 0\ 0]^T$, $v_d = [0\ 0\ 0]^T$, $\Psi_d = [0\ 0\ 0]^T$. The parameters for controller composition are shown in Table 1. The desired orbital elements are shown in Table 2 [30]. The disturbance input of the system are $d_i = [d_{\Psi_i}^T\ d_{v_i}^T]^T$ are assumed as [31]

$$d_{\Psi i} = \begin{bmatrix} 1 + \sin(\pi t/125) + \sin(\pi t/200) \\ 1 - \sin(\pi t/125) - \sin(\pi t/200) \\ 1 + \cos(\pi t/125) + \cos(\pi t/200) \end{bmatrix} \times 10^{-5} N \cdot m \tag{67}$$

and

$$d_{vi} = \begin{bmatrix} 1 + \sin(\pi t/125) + \sin(\pi t/200) \\ 1 - \sin(\pi t/125) - \sin(\pi t/200) \\ 1 + \cos(\pi t/125) + \cos(\pi t/200) \end{bmatrix} \times 10^{-4} N \tag{68}$$

B. FORMATIONS OF SPACECRAFT RESULT ANALYSIS

The simulation results are shown in Figures 3-12. Figures 3-4 show the attitude of four spacecrafts. Figures 5-8 position error function evolution and the configuration error vector of four spacecrafts. Figures 9 to 12 display the torque and force profiles with and without the saturation controller.

By observing Figure 3 and Figure 4, it is evident that the evolution of the error function for S1 spacecraft's attitude, denoted as φ_{R_1}, tends to zero within 25 seconds, while the position error φ_{p_1} tends to zero within 20 seconds. For the result of the error function evolution of S2 spacecraft attitude φ_{R_2} and position φ_{p_2}, it can be seen that φ_{R_2} and φ_{p_2} were disturbed during the convergence process, but then converged in a short time. Then, the S3 spacecraft attitude φ_{R_3} tend to zero in 60s and positionφ_{p_3} tend to zero in 50s. It can be seen from the figure that the error convergence time is longer than S2, but the convergence is completed within 60s. For the attitude and position error function evolution and the configuration error vector of spacecraft S4. Since S4 obtains the attitude of S3 through the observer to control its own

TABLE 1. Control parameters chosen for numerical analysis.

Parameter Name	Value
k_1	0.5
k_2	0.5
k_3	0.5
k_4	1
$K_i\ (i = 1, 2, 3, 4)$	2
$\varepsilon_i (i = 1, 2, 3, 4)$	0.01
ω_{11}	$[\ 0.08\ \ 0.08\ \ 0.08\ \ 8\ \ 8\ \ 8\ ]^T$
ω_{12}	$[\ 0.8\ \ 0.8\ \ 0.8\ \ 8\ \ 8\ \ 8\ ]^T$
ω_{13}	$[\ 0.8\ \ 0.8\ \ 0.8\ \ 8\ \ 8\ \ 8\ ]^T$
ω_{14}	$[\ 10\ \ 10\ \ 10\ \ 10\ \ 10\ \ 10\ ]^T$
γ_{11}	$[\ 0.4\ \ 0.4\ \ 0.1\ \ 4\ \ 4\ \ 4\ ]^T$
γ_{12}	$[\ 0.06\ \ 0.6\ \ 0.06\ \ 0.6\ \ 0.6\ \ 0.6\ ]^T$
γ_{13}	$[\ 0.6\ \ 0.6\ \ 0.15\ \ 6\ \ 6\ \ 6\ ]^T$
γ_{14}	$[\ 1.7\ \ 17\ \ 1.7\ \ 17\ \ 17\ \ 17\ ]^T$

TABLE 2. Desired orbital elements of the leader.

Orbital elements	Values
Semi-major axis (km)	6971
Eccentricity	0.02
Inclination (°)	30
Longitude ascending node (°)	45
Argument of perigee (°)	30
Initial true anomaly (°)	0
Gravitational constant (m^3/s^2)	3.986×10^{14}

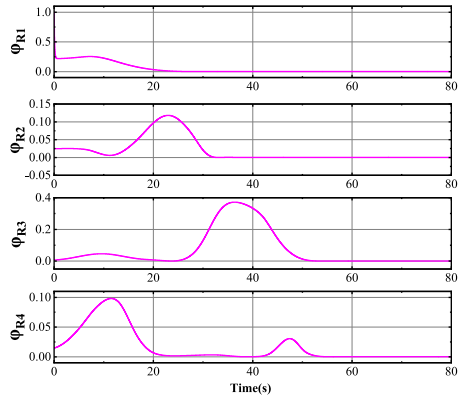

FIGURE 3. The attitude error function evolution of S1 - S4.

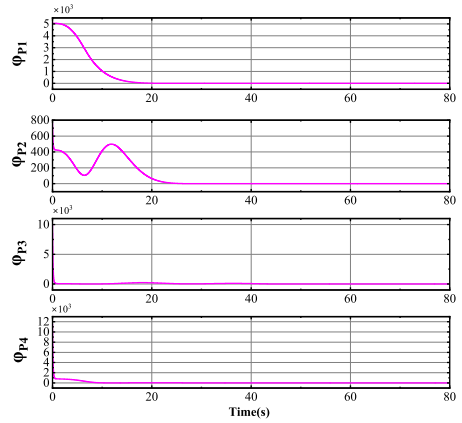

FIGURE 4. The position error function evolution of S1 - S4.

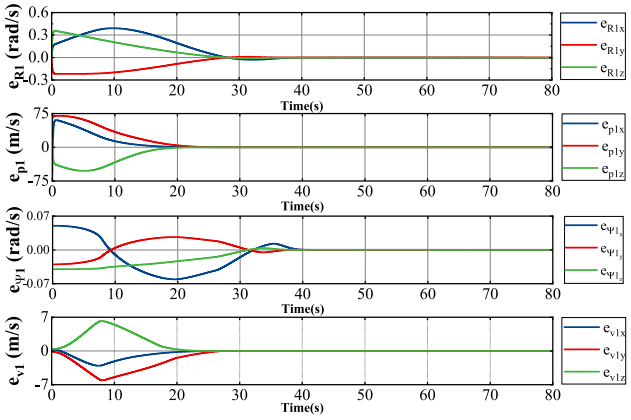

FIGURE 5. The configuration error vector of S1.

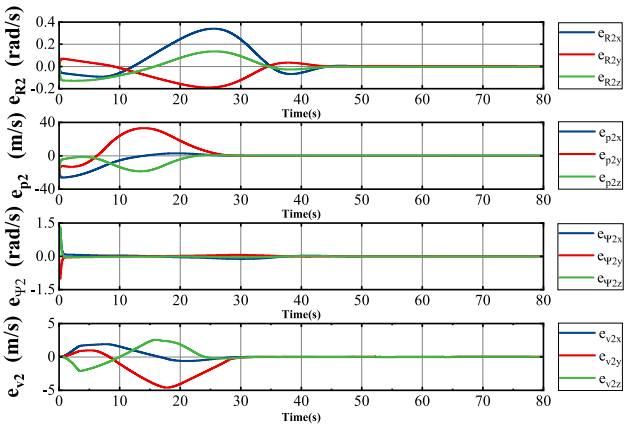

FIGURE 6. The configuration error vector of S2.

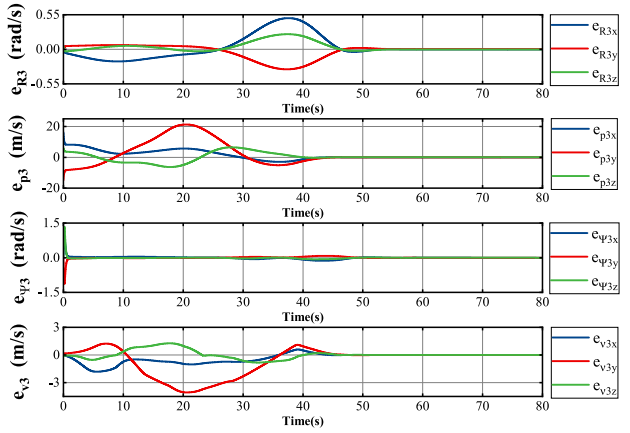

FIGURE 7. The configuration error vector of S3.

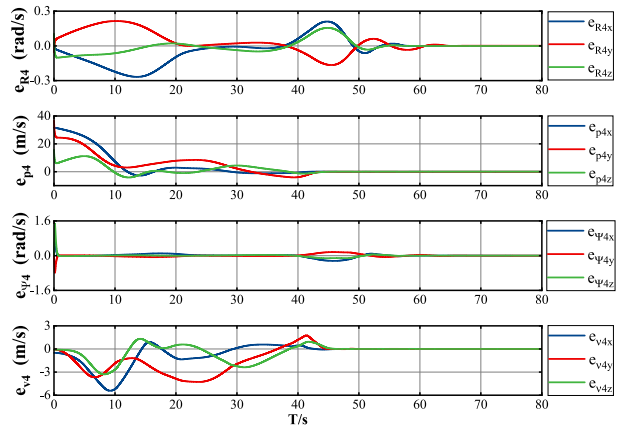

FIGURE 8. The configuration error vector of S4.

attitude, it can be seen that when the attitude of S3 changes greatly, the attitude of S4 will also change accordingly.

As a result, the attitude and position error function evolution and the configuration error vector of four spacecrafts can all converge in a finite time, the four spacecrafts form a formation in a relatively short period of time.

Figure 9 displays the input torque and input force of S1, where M_{U1} and F_{U1} have constraint controllers, M_1 and F_1 have no constraint controllers. For input torque M_{U1}, the upper and lower limit intervals on the x, y, z axis are $[-0.1, 0.05]$, $[-0.02, 0.03]$, $[-0.03, 0.06]$ respectively. It can be seen that the torque with asymmetric input constraints all change within a limited range, and the convergence time is only extended by less than 5s compared

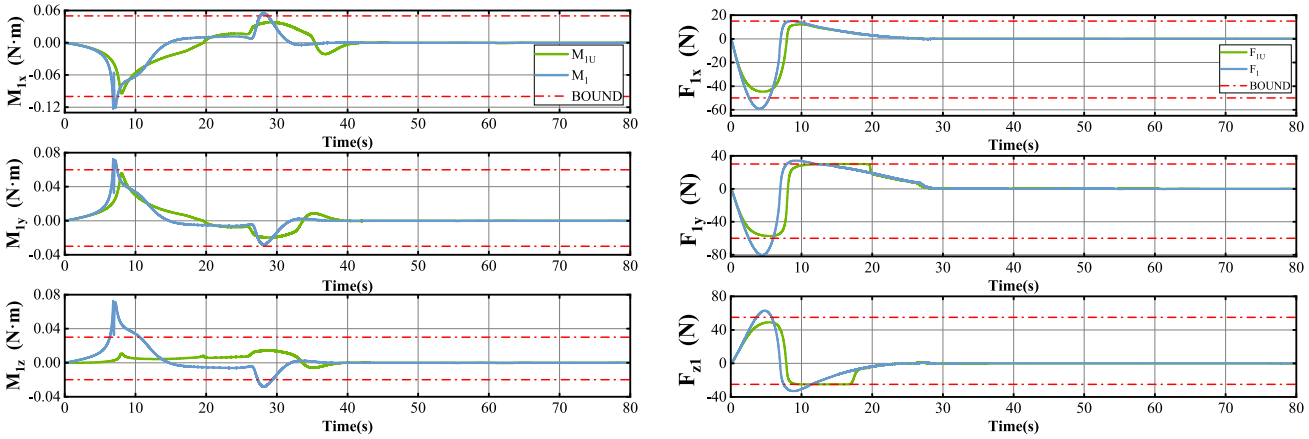

(a)Torque of S1 (b)Force of S1

FIGURE 9. The torque M_{1x}, M_{1y}, M_{1z} and force F_{1x}, F_{1y}, F_{1z} of S1 spacecraft with control law.

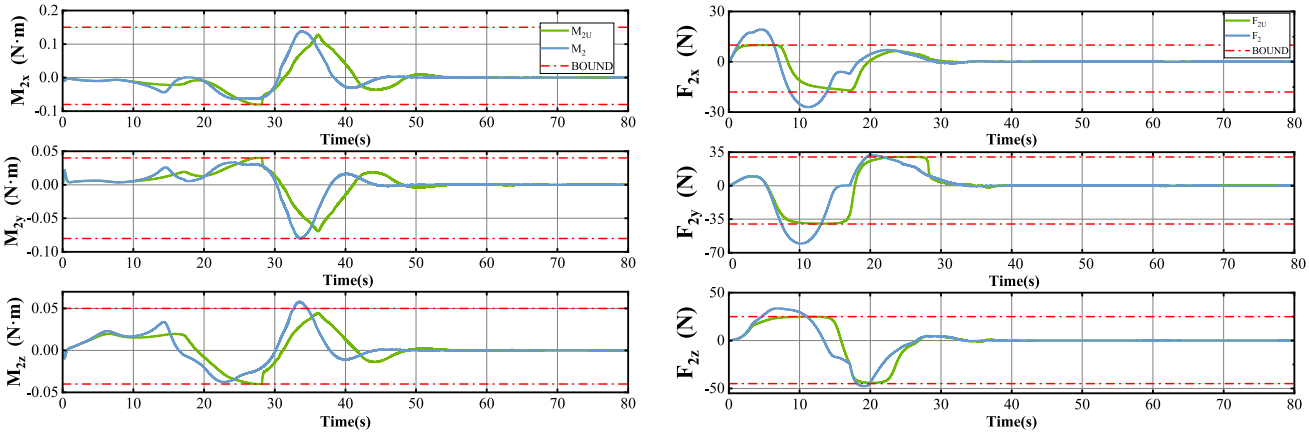

(a)Torque of S2 (b)Force of S2

FIGURE 10. The torque M_{2x}, M_{2y}, M_{2z} and force F_{2x}, F_{2y}, F_{2z} of S2 spacecraft with control law.

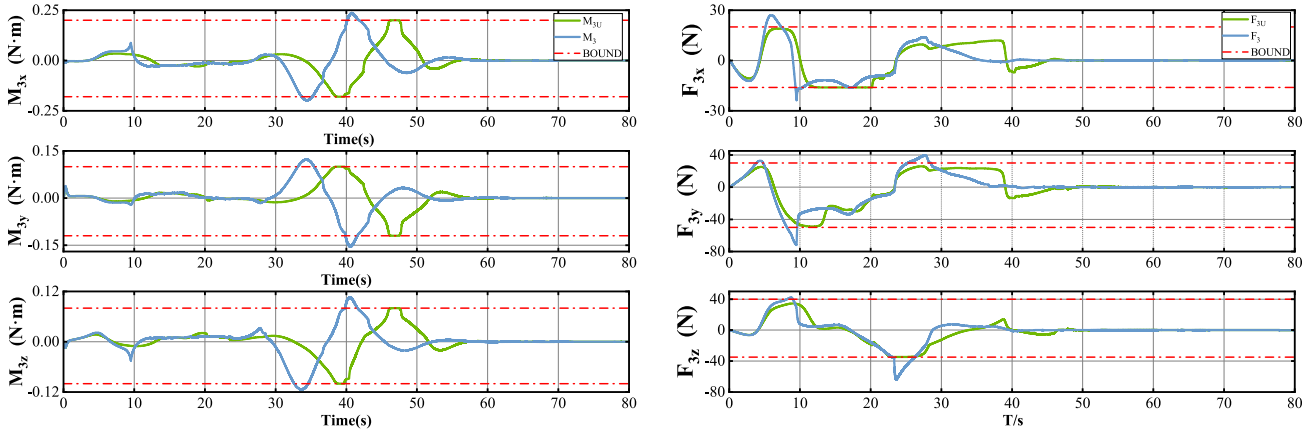

(a)Torque of S3 (b)Force of S3

FIGURE 11. The torque M_{3x}, M_{3y}, M_{3z} and force F_{3x}, F_{3y}, F_{3z} of S3 spacecraft with control law.

with the torque without constraints, and the convergence is completed within 40s. For the force F_{U1}, the upper and lower limit intervals set by x, y, z are $[-50, 15]$, $[-60, 30]$, $[-25, 55]$ respectively. The figure demonstrates that F_{U1} remains within the specified limit range, and all variables achieve convergence within a 30-second timeframe.

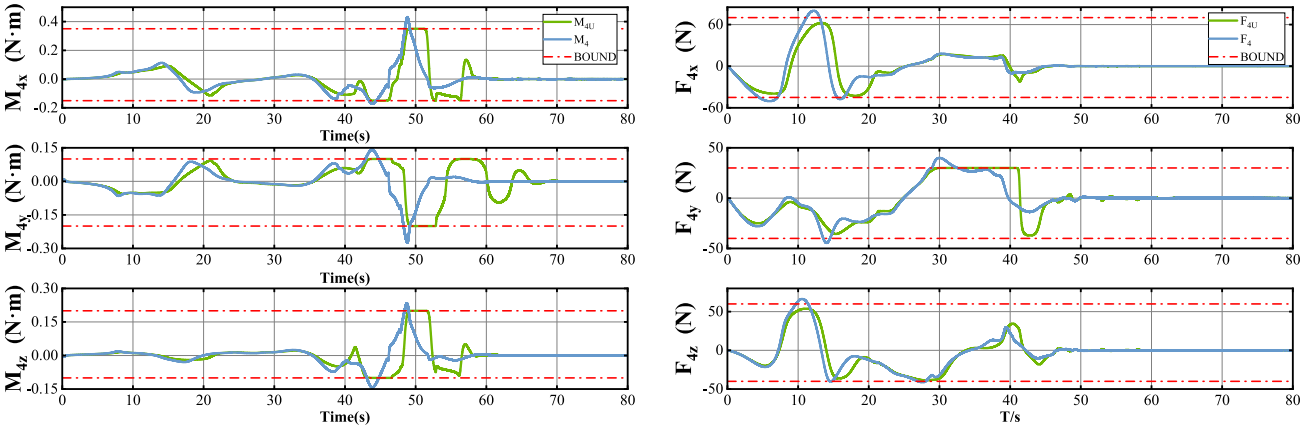

(a)Torque of S4 (b)Force of S4

FIGURE 12. The torque M_{4x}, M_{4y}, M_{4z} and force F_{4x}, F_{4y}, F_{4z} of S4 spacecraft with control law.

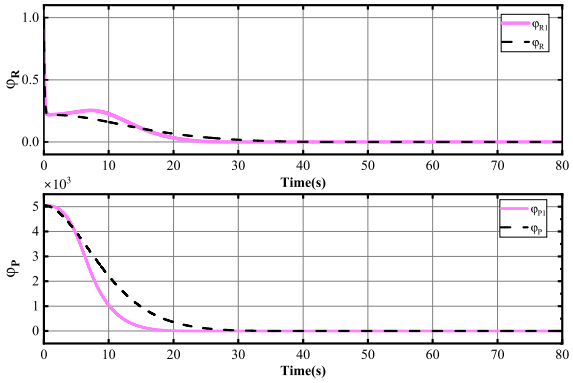

FIGURE 13. The attitude and position error function evolution of spacecraft.

By incorporating a Gaussian error function into the constraint controller, we observe that the transition of the force curve is smoother at corners.

Figures 10-12 demonstrate that both the torque and force converge within the specified constraint range, and the convergence time falls within a limited range. At the same time, it should be pointed out that due to the influence of the formation, the leader will complete the convergence first, and then the follower will complete the convergence, so it can be seen that the time for the four spacecraft to reach a stable state is gradually increasing. Based on the simulation results presented above, we can observe the superiority and the effectiveness of this method for convergence time and control input constraints.

C. SINGLE OF SPACECRAFT RESULT ANALYSIS

The simulation results are shown in Figures 13-15. Figures 13-14 show the attitude and position error function evolution and the configuration error vector of the spacecraft. Figure 15 shows the torque and force with control law.

From Figure 13, it can be seen that under the control law the error function evolution of the spacecraft attitude φ_{R_1} tend to zero in 25s and position φ_{p_1} tend to zero in 20s. While under the sliding mode control the error function evolution of the spacecraft attitude φ_R tends to zero in the 35s and position φ_p tends to zero in the 30s.

From Figure 14, it can be seen that under the control law the error function evolution of the spacecraft translational velocity vectors e_{p_1}, rotation angles vectors e_{R_1}, translational velocity vectors e_{v_1}, rotation angles vectors e_{Ψ_1} converge to small sets around zero in 30s, 40s, 30s, 40s, respectively. While under the sliding mode control the error function evolution of the translational velocity vectors e_p, rotation angles vectors e_R, translational velocity vectors e_v, rotation angles vectors e_Ψ converge to small sets around zero in 40s, 50s, 40s, 50s, respectively. As a result, the proposed scheme fast achieves the control aim for the coupled 6-DOF rigid-body spaceship based on the nonlinear manifold $SE(3)$ model within a finite amount of time.

Figure 15 displays the input torque and input force of the spacecraft, where M_{U1} and F_{U1} have constraint controllers, M_1 and F_1 have no constraint controllers, M and F under the sliding mode control. For input torque M_{U1}, the upper and lower limit intervals on the x, y, z axis are $[-0.1, 0.05]$, $[-0.02, 0.03]$, $[-0.03, 0.06]$ respectively. It can be seen that the torque with asymmetric input constraints all changes within a limited range, and the convergence time is only extended by less than 5s compared with the torque without constraints, and the convergence is completed within the 40s. While under the sliding mode control the convergence is completed within the 50s. For the force F_{U1}, the upper and lower limit intervals set by x, y, z are $[-50, 15]$, $[-60, 30]$, $[-25, 55]$ respectively. It can be seen from the figure that F_{U1} does not exceed the limit range, and all complete the convergence within the 30s. While under the sliding mode control the convergence is completed within the 40s.

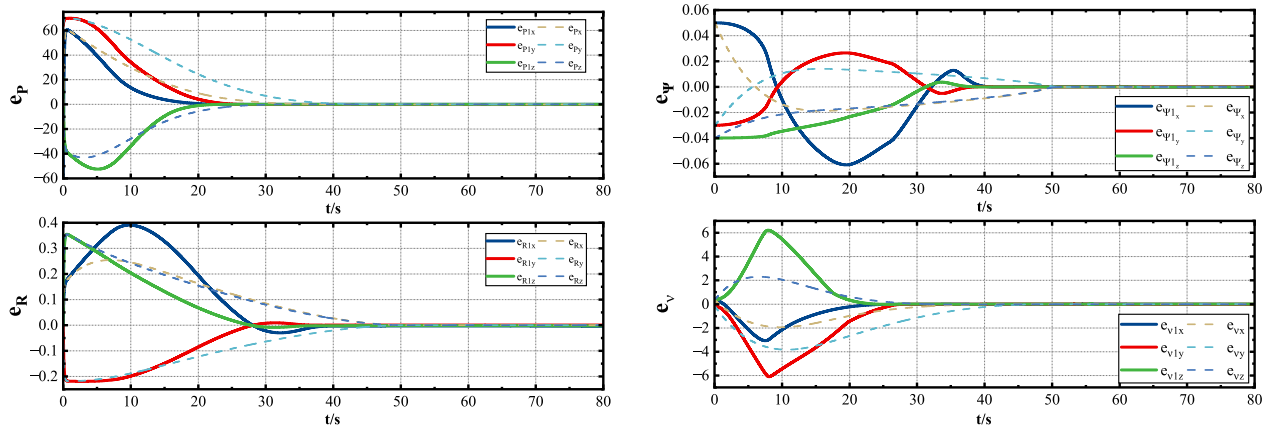

(a) The configuration error vector of spacecraft

(b) The generalized velocity error of spacecraft

FIGURE 14. The spacecraft error function evolution of translational velocity vectors e_P, rotation angles vectors e_R, rotation angles vectors e_Ψ and translational velocity vectors e_v.

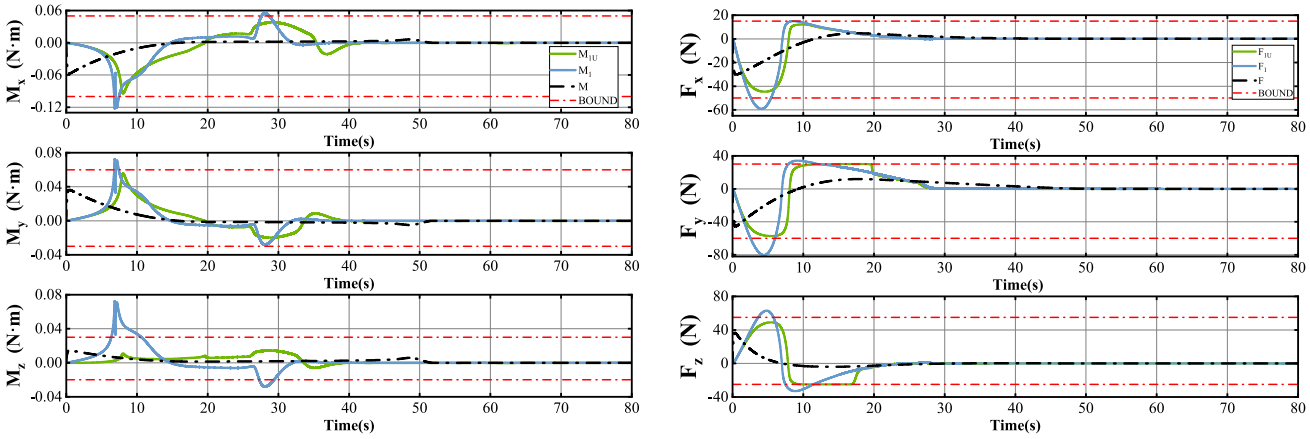

(a) Torque of spacecraft

(b) Force of spacecraft

FIGURE 15. The torque M_x, M_y, M_z and force F_x, F_y, F_z of spacecraft with control law.

From the observations of Figures 13-15, it is evident that both the torque and force converge within the specified constraint range, while the time of convergence remains within a limited range. At the same time, it should be pointed out that under the control law convergence is faster. Based on the simulation results presented above, we can observe the superiority and the effectiveness of the method in this paper for convergence time and control input constraints.

V. CONCLUSION

For distributed spacecraft systems, an asymmetric saturation control strategy based on SE3 is proposed. A new configuration error function is designed on $SE(3)$, and the configuration error vector is derived from the configuration function. Using a novel asymmetric saturable actuator, we have designed a distributed adaptive spacecraft formation controller. This controller ensures that the spacecraft formation can stabilize to the desired position within a finite time, even in the presence of multiple disturbances and thrust constraints. Lyapunov stability analysis demonstrates the fixed-time stability of the proposed control scheme. Simulation results verify the effectiveness of the method in this paper, showcasing its good performance. This controller provides an alternative method for spacecraft formation under asymmetric constraints and can be extended to many other autonomous aircrafts.

APPENDIX A PROOF OF OBSERVER

Firstly, the observer error is formulated as follows:

$$\begin{cases} e_g\left(g_j, \hat{g}_j\right) = \begin{bmatrix} e_R\left(R_j, \hat{R}_j\right) \\ e_p\left(p_j, \hat{p}_j\right) \end{bmatrix} \\ e_\zeta\left(\zeta_j, \hat{\zeta}_j\right) = \hat{\zeta}_j - \zeta_j \end{cases} \tag{A.1}$$

The sliding mode surface is set as: $s = e_\zeta\left(\zeta_j, \hat{\zeta}_j\right) + n_0 e_g\left(g_j, \hat{g}_j\right)$, when,$s = 0$, there is

$$e_\zeta\left(\zeta_j, \hat{\zeta}_j\right) = -n_0 e_g\left(g_j, \hat{g}_j\right) \tag{A.2}$$

Lyapunov function $V = \varphi_g\left(g_j, \hat{g}_j\right)$ was selected to prove stability.

Then, there are:

$$\begin{aligned}
\varphi_g\left(g_j, \hat{g}_j\right) &= \varphi_R\left(R_j, \hat{R}_j\right) + \varphi_p\left(p_j, \hat{p}_j\right) \\
\varphi_R\left(R_j, \hat{R}_j\right) &= 2 - \sqrt{1 + tr\left(\hat{R}_j^T R_j\right)} \\
\varphi_p\left(p_j, \hat{p}_j\right) &= \frac{1}{2}\left\|p_j - \hat{p}_j\right\|^2
\end{aligned} \tag{A.3}$$

$$\begin{aligned}
\dot{V} &= e_g\left(g_j, \hat{g}_j\right) \cdot e_\zeta\left(\zeta_j, \hat{\zeta}_j\right) \\
&= e_g\left(g_j, \hat{g}_j\right) \cdot \left(-n_0 e_g\left(g_j, \hat{g}_j\right)\right) \\
&= -n_0\left\|e_g\left(g_j, \hat{g}_j\right)\right\|^2
\end{aligned} \tag{A.4}$$

According to (62), $\left\|e_g\left(g_j, \hat{g}_j\right)\right\|^2 \geqslant \frac{1}{2}V$. So there is $\dot{V} \leqslant -\frac{1}{2}n_0 V$. Thus, the observer is stable when the sliding mode surface is $s = 0$.

The design observer gain n is proved as follows: When $k e_g\left(g_j, \hat{g}_j\right) > \Pi^{-1}\left(ad^*_{\hat{\zeta}_j}\Pi\hat{\zeta}_j - ad^*_{\zeta_j}\Pi\zeta_j + s + n_0\dot{e}_g\left(g_j, \hat{g}_j\right)\right)$, the sliding mode surface s will converge to 0. The Lyapunov function $V_s = \frac{1}{2}s^T s$ is chosen to prove its stability, then there are:

$$\begin{aligned}
\dot{V}_s &= s^T\dot{s} \\
&= s^T\left(\dot{e}_\zeta\left(\zeta_j, \hat{\zeta}_j\right) + n_0\dot{e}_g\left(g_j, \hat{g}_j\right)\right) \\
&= s^T\left(\Pi^{-1}\left(-k e_g\left(g_j, \hat{g}_j\right) + ad^*_{\hat{\zeta}_j}\Pi\hat{\zeta}_j - ad^*_{\zeta_j}\Pi\zeta_j\right)\right. \\
&\quad \left. + n_0\dot{e}_g\left(g_j, \hat{g}_j\right)\right)
\end{aligned} \tag{A.5}$$

because of $k e_g\left(g_j, \hat{g}_j\right) > \Pi\left(s + n_0\dot{e}_g\left(g_j, \hat{g}_j\right)\right) + ad^*_{\hat{\zeta}_j}\Pi\hat{\zeta}_j - ad^*_{\zeta_j}\Pi\zeta_j$, there is

$$\begin{aligned}
&s^T\left(\Pi^{-1}\left(\begin{array}{c}-k e_g\left(g_j, \hat{g}_j\right) + ad^*_{\hat{\zeta}_j}\Pi\hat{\zeta}_j - \\ ad^*_{\zeta_j}\Pi\zeta_j \\ k_1\dot{e}_g\left(g_j, \hat{g}_j\right)\end{array}\right) + \right) \\
&< s^T\left(\Pi^{-1}\left(\begin{array}{c}\Pi\left(-s - n_0\dot{e}_g\left(g_j, \hat{g}_j\right)\right) - \\ ad^*_{\hat{\zeta}_j}\Pi\hat{\zeta}_j + ad^*_{\zeta_j}\Pi\zeta_j + \\ ad^*_{\hat{\zeta}_j}\Pi\hat{\zeta}_j - ad^*_{\zeta_j}\Pi\zeta_j \\ n_0\dot{e}_g\left(g_j, \hat{g}_j\right)\end{array}\right) + \right) \\
&= -s^T s \\
&< 0
\end{aligned} \tag{A.6}$$

Therefore, $\dot{V}_s < 0$, then s is going to converge to 0. At this point, the proof of the observer is complete.

REFERENCES

[1] P. Huang, Y. Hu, Y. Zhao, J. Ma, F. Zhang, Z. Meng, and Z. Liu, "Coordinated formation control strategy of the rotating hub-spoke tethered formation system," *Proc. Inst. Mech. Eng., G, J. Aerosp. Eng.*, vol. 232, no. 2, pp. 317–330, Feb. 2018, doi: 10.1177/0954410016683729.

[2] M.-L. Zhuang and S.-M. Song, "Fixed-time coordinated attitude tracking control for spacecraft formation flying considering input amplitude constraint," *Int. J. Control, Autom. Syst.*, vol. 20, no. 7, pp. 2129–2147, Jul. 2022, doi: 10.1007/s12555-021-0366-8.

[3] L. Chen, Q. Yang, C. Li, and G. Ma, "Controlling dynamic formations of mobile agents governed by Euler–Lagrange dynamics," *Int. J. Control, Autom. Syst.*, vol. 19, no. 5, pp. 1740–1750, May 2021, doi: 10.1007/s12555-020-0274-3.

[4] J. K. Zhou, G. F. Ma, and Q. L. Hu, "Delay depending decentralized adaptive attitude synchronization tracking control of spacecraft formation," *Chin. J. Aeronaut.*, vol. 25, no. 3, pp. 406–415, 2012, doi: 10.1016/S1000-9361(11)60404-4.

[5] D. Li, S. S. Ge, G. Ma, and W. He, "Layered formation-containment control of multi-agent systems in constrained space," *Int. J. Control, Autom. Syst.*, vol. 18, no. 3, pp. 768–779, Mar. 2020, doi: 10.1007/s12555-019-0172-8.

[6] H. Du, B. Yu, J. Wei, J. Zhang, D. Wu, and W. Tao, "Attitude trajectory planning and attitude control for quad-rotor aircraft based on finite-time control technique," *Appl. Math. Comput.*, vol. 386, Dec. 2020, Art. no. 125493, doi: 10.1016/j.amc.2020.125493.

[7] W. H. Clohessy and R. S. Wiltshire, "Terminal guidance system for satellite rendezvous," *J. Aerosp. Sci.*, vol. 27, no. 9, pp. 653–658, Sep. 1960, doi: 10.2514/8.8704.

[8] H. Wong, H. Pan, and V. Kapila, "Output feedback control for spacecraft formation flying with coupled translation and attitude dynamics," in *Proc. Amer. Control Conf.*, Jun. 2005, pp. 2419–2426, doi: 10.1109/ACC.2005.1470329.

[9] P. K. C. Wang and F. Y. Hadaegh, "Terminal guidance system for satellite rendezvous," *J. Astron. Sci.*, vol. 44, pp. 315–355, Jun. 1996.

[10] J. Qiao, D. Zhang, Y. Zhu, and P. Zhang, "Disturbance observer-based finite-time attitude maneuver control for micro satellite under actuator deviation fault," *Aerosp. Sci. Technol.*, vols. 82–83, pp. 262–271, Nov. 2018, doi: 10.1016/j.ast.2018.09.007.

[11] S. Li, C. Liu, and Z. Sun, "Finite-time distributed hierarchical control for satellite cluster with collision avoidance," *Aerosp. Sci. Technol.*, vol. 114, Jul. 2021, Art. no. 106750, doi: 10.1016/j.ast.2021.106750.

[12] Q. Hu and X. Shao, "Smooth finite-time fault-tolerant attitude tracking control for rigid spacecraft," *Aerosp. Sci. Technol.*, vol. 55, pp. 144–157, Aug. 2016, doi: 10.1016/j.ast.2016.05.019.

[13] Z. Meng, W. Ren, and Z. You, "Distributed finite-time attitude containment control for multiple rigid bodies," *Automatica*, vol. 46, no. 12, pp. 2092–2099, Dec. 2010, doi: 10.1016/j.automatica.2010.09.005.

[14] C. Zhang, J. Wang, D. Zhang, and X. Shao, "Fault-tolerant adaptive finite-time attitude synchronization and tracking control for multi-spacecraft formation," *Aerosp. Sci. Technol.*, vol. 73, pp. 197–209, Feb. 2018, doi: 10.1016/j.ast.2017.12.004.

[15] H. Gao, Y. Xia, J. Zhang, and B. Cui, "Finite-time fault-tolerant output feedback attitude control of spacecraft formation with guaranteed performance," *Int. J. Robust Nonlinear Control*, vol. 31, no. 10, pp. 4664–4688, Jul. 2021, doi: 10.1002/rnc.5504.

[16] A.-M. Zou and K. D. Kumar, "Quaternion-based distributed output feedback attitude coordination control for spacecraft formation flying," *J. Guid., Control, Dyn.*, vol. 36, no. 2, pp. 548–556, Mar. 2013, doi: 10.2514/1.56352.

[17] X. Sun, X. Wu, W. Chen, Y. Hao, K. A. Mantey, and H. Zhao, "Dual quaternion based dynamics modeling for electromagnetic collocated satellites of diffraction imaging on geostationary orbit," *Acta Astronautica*, vol. 166, pp. 52–58, Jan. 2020, doi: 10.1016/j.actaastro.2019.10.015.

[18] N. Filipe and P. Tsiotras, "Adaptive position and attitude-tracking controller for satellite proximity operations using dual quaternions," *J. Guid., Control, Dyn.*, vol. 38, no. 4, pp. 566–577, Apr. 2015, doi: 10.2514/1.g000054.

[19] S. Li, H. Zou, D. Shi, and J. Wang, "Event-triggered moving horizon pose estimation for spacecraft systems," *J. Beijing Inst. Technol. English Ed.*, vol. 31, no. 4, p. 9, 2022.

[20] Q. Sun and Y. Jia, "Integrated attitude-orbit control for spacecraft proximity operations based on dual quaternion," in *Proc. 41st Chin. Control Conf. (CCC)*, Jul. 2022, pp. 3293–3298, doi: 10.23919/CCC55666.2022.9901657.

[21] L. Wang, Y. Guo, G. Ma, and H. Zhang, "Artificial potential function based spacecraft proximity maneuver 6-DOF control under multiple pyramid-type constraints," *ISA Trans.*, vol. 126, pp. 316–325, Jul. 2022, doi: 10.1016/j.isatra.2021.08.003.

[22] X. Shi, X. Peng, and Y. Gong, "Immersion and invariance adaptive control for spacecraft pose tracking via dual quaternions," *Complexity*, vol. 2021, pp. 1–18, Apr. 2021, doi: 10.1155/2021/6624222.

[23] Y. N. Chelnokov, "Controlling the spatial motion of a rigid body using biquaternions and dual matrices," *Mech. Solids*, vol. 56, no. 1, pp. 13–33, Jan. 2021, doi: 10.3103/s0025654421010064.

[24] S. P. Bhat, and D. S. Bernstein, "A topological obstruction to continuous global stabilization rotational motion unwinding phenomenon," *Syst. Control Lett.*, vol. 39, no. 1, pp. 63–70, 2000, doi: 10.1016/S0167-6911(99)00090-0.

[25] Z. Zhu, Y. Xia, and M. Fu, "Attitude stabilization of rigid spacecraft with finite-time convergence," *Int. J. Robust Nonlinear Control*, vol. 21, no. 6, pp. 686–702, Apr. 2011, doi: 10.1002/rnc.1624.

[26] J. Zhang, D. Ye, Z. Sun, and C. Liu, "Extended state observer based robust adaptive control on SE(3) for coupled spacecraft tracking maneuver with actuator saturation and misalignment," *Acta Astronautica*, vol. 143, pp. 221–233, Feb. 2018, doi: 10.1016/j.actaastro.2017.11.034.

[27] K. Ghasemi, J. Ghaisari, and F. Abdollahi, "Robust formation control of multiagent systems on the lie group $SE(3)$," *Int. J. Robust Nonlinear Control*, vol. 30, no. 3, pp. 966–998, Feb. 2020, doi: 10.1002/rnc.4806.

[28] B. Xiao, X. Yang, and X. Huo, "A novel disturbance estimation scheme for formation control of ocean surface vessels," *IEEE Trans. Ind. Electron.*, vol. 64, no. 6, pp. 4994–5003, Jun. 2017, doi: 10.1109/TIE.2016.2622219.

[29] D. Lee, A. Sanyal, E. Butcher, and D. Scheeres, "Finite-time control for spacecraft body-fixed hovering over an asteroid," *IEEE Trans. Aerosp. Electron. Syst.*, vol. 51, no. 1, pp. 506–520, Jan. 2015, doi: 10.1109/TAES.2014.140197.

[30] D. Lee and G. Vukovich, "Robust adaptive terminal sliding mode control on SE(3) for autonomous spacecraft rendezvous and docking," *Nonlinear Dyn.*, vol. 83, no. 4, pp. 2263–2279, Mar. 2016, doi: 10.1007/s11071-015-2479-1.

[31] X. Xue, X. Yue, and J. Yuan, "Connectivity preservation and collision avoidance control for spacecraft formation flying in the presence of multiple obstacles," *Adv. Space Res.*, vol. 67, no. 11, pp. 3504–3514, Jun. 2021, doi: 10.1016/j.asr.2020.05.036.

[32] Y. Wang, H. Hong, J. Guo, X. Wang, and W. Shang, "Configuration error function design and application to fixed-time geometric terminal sliding-mode control on $SE(3)$," *Acta Astronautica*, vol. 174, pp. 61–71, Sep. 2020.

[33] Z. Yao, X. Liang, G.-P. Jiang, and J. Yao, "Model-based reinforcement learning control of electrohydraulic position servo systems," *IEEE/ASME Trans. Mechatronics*, vol. 28, no. 3, pp. 1446–1455, Jun. 2023.

[34] Y. Wan, S. Chen, L. Yuan, C. Zhang, Y. Zhang, and G. Yang, "Modeling and synchronized control of a dual-drive 'Checkerboard' gantry with composite adaptive feedforward and RISE feedback," *IEEE/ASME Trans. Mechatronics*, vol. 27, no. 4, pp. 2044–2052, Aug. 2022.

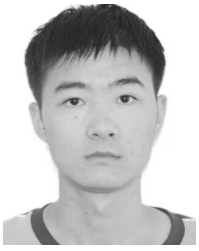

CHAOBO LI is currently pursuing the B.Eng. degree with the Hubei University of Technology (HBUT), Wuhan. Currently, his research under the supervision of Dr. Wei Shang. He has completed a few projects in the fields of adaptive control and stability analysis.

XIAOKANG PENG received the master's degree in aerospace science and technology from the Beijing Institute of Technology, in 2015. He is currently an Engineer with the Shanghai Mechanical and Electrical Engineering Institute. His research interests include guidance law design and optimal control theory.

WEI SHANG received the Ph.D. degree in aeronautical and astronautical science and technology from the Beijing Institute of Technology, China, in 2017. He is currently a Lecturer with the Hubei University of Technology. His research interests include control theory of multi-agent systems and flight control.

YUHAN ZOU is currently pursuing the Bachelor of Engineering degree with the Hubei University of Technology (HBUT), Wuhan, under the supervision of Dr. Wei Shang. She helped complete a few projects in the fields of formation control, stability analysis, and super-twisting.

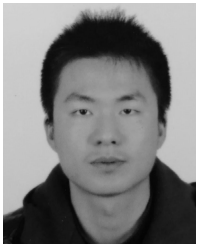

TIANLONG CHEN is currently pursuing the Bachelor of Engineering degree with the Hubei University of Technology (HBUT), Wuhan. Currently, his research under the supervision of Dr. Wei Shang. He helped complete lots of jobs of quadrotor, which include distributed control, nested adaptive, and trajectory tracking.